Title

Naturalistic viewing: An open-access dataset using simultaneous EEG-fMRI

Authors

Qawi K Telesford[1,*], Eduardo Gonzalez-Moreira[1], Ting Xu[2], Yiwen Tian[1], Stanley Colcombe[1], Jessica Cloud[1], Brian Edward Russ[1], Arnaud Falchier[1], Maximilian Nentwich[3], Jens Madsen[3], Lucas Parra[3], Charles Schroeder[1], Michael Milham[1,2], Alexandre Rosa Franco[1,2,*]

Affiliations

[1] Nathan Kline Institute

[2] Child Mind Institute

[3] City College of New York

[*] Corresponding Authors. QKT: qawi.telesford@nki.rfmh.org , ARF: alexandre.franco@nki.rfmh.org

Abstract

In this work we present a dataset that combines functional magnetic imaging (fMRI) and electroencephalography (EEG) to use as a resource for the understanding of human brain function. The dataset can also be used for optimizing preprocessing methods for simultaneously collected imaging data. The dataset includes simultaneously collected recordings from 22 individuals (ages: 23-51) across various visual and naturalistic stimuli. In addition, physiological, eye tracking, electrocardiography, and cognitive and behavioral data were collected along with this neuroimaging data. Visual tasks include a flickering checkerboard that was collected outside and inside the MRI scanner (EEG-only) and simultaneous EEG-fMRI recordings. Simultaneous recordings also included rest, the visual paradigm Inscapes, and several short video movies representing naturalistic stimuli. We present this dataset as part of an effort to provide open-access data with the goal of increasing the opportunity for discoveries and understanding of the human brain and evaluating the correlation between electrical brain activity and blood oxygen level-dependent (BOLD) signals.

Introduction

Simultaneous collection of electroencephalography (EEG) and functional magnetic resonance imaging (fMRI) data is an attractive approach to imaging as it combines the higher spatial resolution of fMRI with the higher temporal resolution of EEG. Combining modalities allows researchers to integrate spatial and temporal information while overcoming the limitations encountered with a single imaging modality (Mele *et al.*, 2019; Nentwich *et al.*, 2020). Nevertheless, the collection of multimodal data simultaneously requires specific expertise and

researchers must overcome a variety of technical challenges to successfully collect data. Such challenges may limit its broader usage in the research community.

There are several technical challenges encountered when collecting several imaging modalities simultaneously. With EEG, the main challenge is due to various sources of noise that impact the recorded signal. Gradient artifact is the greatest source of noise in simultaneous recordings, caused by the magnetic field gradients during fMRI acquisition, which induce current into EEG electrodes (Allen, Josephs and Turner, 2000). Another source of noise is the ballistocardiogram (BCG) signal, which captures the ballistic forces of blood in the cardiac cycle (Yan *et al.*, 2009; Luo, Huang and Glover, 2014). The BCG artifact arises from the pulsation of arteries in the scalp that causes movement in EEG electrodes and generates voltage. In a large magnetic field, the BCG artifact is more pronounced and increases with field strength (Neuner *et al.*, 2014). In addition to gradient and BCG artifacts, other sources of noise include the MRI helium compressor (van der Meer *et al.*, 2016), eye blinks (Hoffmann and Falkenstein, 2008), head movement, and respiratory artifacts (Power *et al.*, 2019). Collecting simultaneous fMRI and EEG requires overcoming a variety of technical challenges, but also need advanced preprocessing techniques to overcome these unavoidable artifacts and produce a clean signal. In this paper, we detail how we addressed various technical challenges encountered including strategies used to improve data quality.

For this dataset, the majority of the tasks performed by the participants are naturalistic viewing tasks. Naturalistic stimuli represent paradigms that are considered more complex and dynamic than task-based stimuli (Fishell *et al.*, 2019; Zhang *et al.*, 2021). Naturalistic viewing provides more physiologically relevant conditions and produces closer to real-world brain responses (Sonkusare, Breakspear and Guo, 2019; Nastase, Goldstein and Hasson, 2020; Saarimäki, 2021). Naturalistic stimuli also contain narrative structure and provide context that reflects real-life experiences (Goldberg, Preminger and Malach, 2014; Saarimäki, 2021). Moreover, movies have been found to have high intersubject correlation and reliability (Hasson, Furman, *et al.*, 2008; Yang *et al.*, 2021), holds subjects' attention (Hasson, Landesman, *et al.*, 2008), and improves compliance related to motion and wakefulness (Vanderwal *et al.*, 2015). Naturalistic movies are also an ideal stimulus for multimodal data sets and may be useful in linking responses across levels (Park *et al.*, 2017, 2022) and species (Mantini *et al.*, 2012).

In this manuscript, we present a dataset collected at the Nathan Kline Institute for Psychiatric Research in Orangeburg, NY, representing a study using simultaneously collected EEG and fMRI in healthy adults. The dataset contains multiple scan conditions, including a visual task, resting state, and naturalistic stimuli. We also present quality control metrics for both modalities and provide a detailed description of preprocessing steps used to clean up the EEG data. Lastly, we openly share these raw and processed data through the International Neuroimaging Data-Sharing Initiative (INDI) and along with preprocessing code.

Methods

Participants and procedures

Simultaneous EEG-fMRI was collected in twenty-two adults (ages 23–50 years; mean age: 36.8; 50% male) recruited from the Orangeburg, NY community. Participants enrolled in this study have no history of psychiatric illness. All imaging was collected using a 3T Siemens TrioTim equipped with a 12-channel head coil. EEG data were collected using an MR-compatible system by Brain Products consisting of the BrainCap MR with 64 channels, two 32-channel BrainAmp MR amplifiers, and PowerPack battery. Cortical electrodes were arranged according to the international 10-10 system. Inside the scanner, eye tracking was collected using the EyeLink 1000 Plus.

Participants attended two sessions varying between 2 and 354 days between scans (time between scans, mean: 38.2 days; median: 11 days); see Table 1 for breakdown data acquired during sessions. The scanning protocol consisted of three recording conditions. The “Outside” condition was EEG recordings collected outside the MRI scanner in a non-shielded room; the “Scanner OFF” condition consisted of EEG recordings collected inside the static field of the MRI scanner while the scanner was off; the “Scanner ON" condition consisted the simultaneous EEG and fMRI recordings. All research performed was approved by the Institutional Review Board. Prior to the experiment, written informed consent was obtained from all participants. Participants also provided demographic information and behavioral data, including information on their last month of sleep (Pittsburgh Sleep Study) (Buysse *et al.*, 1989), the amount of sleep they had the previous night, and their caffeine intake, if any, before the scan session.

Session	Recording Location	Scan	Run Length (s)
Day 1	Outside	Checkerboard (12Hz)	200
	Scanner OFF	Checkerboard (12Hz)	200
	Scanner ON	Checkerboard (12Hz)	200
		Rest	600
		Inscapes	600
		The Present [Run 1]	258
		PEER	90
		Monkey 1 [Run 1]	300
		Despicable Me (English) [Run 1]	600
		MPRAGE	600
		The Present [Run 2]	258
		Monkey 1 [Run 2]	300
		Despicable Me (English) [Run 2]	600
Day 2	Outside	Checkerboard (12Hz)	200
	Scanner OFF	Checkerboard (12Hz)	200
	Scanner ON	Checkerboard (12Hz)	200
		Rest	600
		Inscapes	600
		Monkey 2 [Run 1]	300
		PEER	90
		Despicable Me (Hungarian) [Run 1]	600
		Monkey 5 [Run 1]	300
		MPRAGE	600
		Monkey 2 [Run 2]	300
		Despicable Me (Hungarian) [Run 2]	600
		Monkey 5 [Run 2]	300

Table 1. Simultaneous EEG-fMRI experimental design. EEG and fMRI were collected simultaneously across two scan sessions.

EEG acquisition

The entire procedure takes approximately three hours. Approximately 45 minutes is spent preparing a participant for EEG. Preparation begins with measuring the participant's head to determine cap size. An anterior to posterior measurement is also taken across the top of the head, from the nasion to inion. A mark is made at the center of the forehead 10% of the measured nasion-inion distance. A proper sized cap is placed on the participant's head with the electrode Fpz centered at the mark on the forehead. Once the subject is fitted with the EEG cap, electrodes are filled with gel. In this study EEG is collected using a customized cap to record 61 cortical channels, two EOG channels placed above (channel 64) and below the left eye (channel 63), and one ECG channel (channel 32) placed on the back. In addition, the cap also contains a reference and ground electrode. Electrodes were filled using V19 Abralyt HiCl electrode gel. Electrode impedance was recorded before every recorded run; to ensure good data quality, electrode impedance was kept below 20kOhm. EEG was recorded using BrainVision Recorder at a sampling rate of 5000Hz. After cap preparation, participants

completed a single run of the flickering checkerboard experiment in a non-shielded room, outside the scanner environment; this run is referred to as the "Outside" scan. After the Outside scan, participants move to the MRI suite. Prior to placement in the MR scanner, a 3D scan of the participant's head is collected to digitize the position of EEG electrodes. 3D scans were collected using a portable scanner, the Occipital Structure Sensor (Occipital Inc, Boulder CO), and iPad Mini 4 (Apple, Cupertino, CA). Due to PHI restrictions, 3D scans will not be available in the data release.

Simultaneous EEG-fMRI recording in the MRI scanner

After 3D digitization, participants enter the MRI scanner and are placed on the scanner bed in the supine position. Cushions are placed around the head to provide stabilization and minimize head motion during scans. At this stage, participants are provided with MR-safe goggles if they have any visual impairment that requires glasses. Participants are also fitted with a respiratory transducer belt to monitor breathing, which was recorded using BIOPAC MP150 (BIOPAC Systems, Inc., Goleta, CA).

Once positioned in the scanner, the participant's head is enclosed in a 12-channel 3T head matrix MR coil. The cable bundle from the EEG cap is routed through the front of the head coil and fixed at the top of the head coil using medical tape. The cable bundles are connected to the amplifiers and battery pack. During EEG data acquisition, the software is synchronized to the master clock of the MRI scanner. During recordings, EEG data was continuously collected along with task onset triggers, and volume triggers were recorded at the beginning of each TR.

Eye tracking acquisition

For recordings collected inside the scanner, eye position and pupil dilation were recorded using an infrared based eye tracker (EyeLink 1000, SR Research Ltd., Ontario, Canada; http://www.sr-research.com) at a sampling rate of 1000Hz. The eye tracker was calibrated using a 9-point grid before recordings in the MRI scanner. Participants were asked to direct their gaze at dots presented on the grid. Calibration was followed by a validation step until the error between the two measurements was less than 1° (SR Research Ltd., 2009).

MRI data acquisition

MRI data was acquired using a 12-channel head coil on 3.0T Siemens TIM Trio. MPRAGE structural T1w images were acquired with the following parameters: TR = 2500ms; TI = 1200ms; TE = 2.5ms; slices = 192; matrix size = 256×256; voxel size = 1mm^3 isotropic; flip angle = 8°; partial Fourier off; pixel bandwidth = 190 Hz/Px. All BOLD fMRI sequences were acquired with these parameters: TR = 2100ms; TE = 24.6ms; slices = 38; matrix size = 64×64; voxel size = 3.469×3.469×3.330 mm. Run length for each task is listed in Table 1.

Task data/stimuli description

In this section, we describe the data generated for this study focused on the collection of simultaneous EEG and fMRI. This dataset consists of task, naturalistic stimuli and resting state data. In addition to the simultaneously collected data, task data was collected outside the MRI

scanner and inside the scanner environment with the scanner off. Collection of this data enables us to assess the impact of changes in the scanning environment on the EEG recordings. EEG-fMRI data was collected across two scan sessions; structural data was collected during the middle of the scan (see Table 1 for details).

Checkerboard stimulus

The use of flickering visual stimuli has been used to investigate the visual system in EEG (Galloway, 1990; Herrmann, 2001) and fMRI (Sun *et al.*, 2014; Bayram *et al.*, 2016). A high-contrast flickering checkerboard task was used to stimulate the primary visual cortical regions. Participants were shown a flickering radial checkerboard at a frequency of 12Hz in 20-second trials following a 20-second rest period across five repetitions. The checkerboard stimulus was presented outside the scanner after cap placement, inside the scanner with the scanner off, and inside scanner during a simultaneous EEG and fMRI. These three recordings were collected to measure the impact of the MRI scanning sequence on the recorded EEG.

Rest

The participant was presented a white fixation cross in the center of a black screen and instructed to rest with eyes open. Participants had one rest scan per session, each scan was 10 minutes.

Inscapes

Inscapes is a computer-generated animation featuring abstract 3D shapes and moves in slow continuous transitions. The video was originally developed as a 7-minute video for children to watch during brain scans with the goal of providing stimulation to keep children engaged while minimizing some cognitive processing that may be engaged (Vanderwal *et al.*, 2015). Participants were presented with an extended version of Inscapes that was 10 minutes in length. Similar to the rest scan, the Inscapes video was viewed once per scan session.

Predictive eye estimation (PEER) calibration

Predictive eye estimation regression (PEER) is an imaging-based calibration scan used to estimate the direction of eye gaze (Son *et al.*, 2020). Participants were told to direct their gaze at dots that appear at random points on the screen. The sequence of randomized locations was the same for all participants. The PEER method estimates eye gaze from the collected scan using support vector regression (SVR), a machine learning algorithm. The algorithm estimates the direction of eye gaze during each repetition (TR) in the fMRI time series to estimate the direction.

Naturalistic stimuli (Movies)

Participants viewed three movies twice in one scan session. Videos varied between 258s and 600s. Naturalistic stimuli included, “The Present” [4m18s] (uploaded to YouTube 7 Feb 2016)

(Frey, 2014), two 10-minute clips from “Despicable Me” [clips taken from Russian Blu-Ray with exact times 1:02:09-1:12:09 (English) and 0:12:12-0:22:12 (Hungarian)] (Alexander *et al.*, 2017), three monkey videos (5m00s) (Russ and Leopold, 2015).

Limitations

The fMRI imaging in this dataset was collected using a 12-channel head coil on a 3T scanner platform. While we possess the ability to scan at 3T with a 32-channel head coil, the head coil design does not allow for the EEG cap cable bundle to be routed perpendicularly from the top of the head. Moreover, the design of the head coil does not permit alternate routing of the cable bundle because it will block the participant’s eyes or the cable length is too short to reach the amplifiers. In this study, the cable bundle is routed through the front and then taped to the top of the head coil before it is connected to the amplifier. Using a 12-channel head coil limited the sequences that could be used to collect fMRI, including the use of multiband sequences. Another limiting factor is that imaging sequences with faster TRs could not be used while collecting data simultaneously. The main issue is a safety concern regarding the deposition of radiofrequency (RF) power that causes heating in the EEG leads and electrodes during a sequence (Egan *et al.*, 2021). In this study, we used a TR of 2100ms to ensure participants were not at risk of burns due to the heating of electrodes.

EEG Preprocessing

We developed an automated pipeline to preprocess all EEG data collected outside and inside the MRI scanner. The preprocessing methods used on the EEG data was dependent on where data was acquired. All EEG data was preprocessed using EEGLAB and associated plugins (Delorme and Makeig, 2004). For data collected inside the scanner, data was preprocessed using the FMRIB plug-in for EEGLAB, provided by the University of Oxford Centre for Functional MRI of the Brain (FMRIB) (Iannetti *et al.*, 2005; Niazy *et al.*, 2005).

For data collected in the Outside condition, the following preprocessing steps were used: 1) bandpass filter using a Hamming windowed sinc FIR filter between 0.5Hz and 70Hz; 2) reference electrodes using average reference, excluding the ECG channel, EOG channels, and electrodes excluded during the EEG quality control process.

For data collected in the Scanner OFF condition, the prior preprocessing steps used in the Outside condition were used; in addition, pulse artifact detection and removal was used due to the increased contamination of the signal caused by participant’s heartbeat (Allen, Josephs and Turner, 2000): 1) QRS/heartbeat detection using the ECG channel; 2) pulse artifact/BCG removal using template subtraction based on the median artifact; 3) bandpass filter using a Hamming windowed sinc FIR filter between 0.5Hz and 70Hz; 4) reference electrodes using average reference, excluding the ECG channel and EOG channels.

For data collected in the Scanner ON condition, the prior preprocessing steps used in the Scanner OFF condition were used; in addition, gradient artifact removal was used to remove the contamination of the EEG signal caused by the changing gradients from the fMRI pulse sequence (Iannetti *et al.*, 2005): 1) gradient artifact removal; 2) QRS/heartbeat detection using

the ECG channel; 3) pulse artifact/BCG removal using template subtraction based on the median artifact; 4) bandpass filter using a Hamming windowed sinc FIR filter between 0.5Hz and 70Hz; 5) reference electrodes using average reference, excluding the ECG channel and EOG channels.

Gradient Artifact Removal

The gradient artifact is the largest source of noise in simultaneous EEG-fMRI data, measuring more than 400 times larger than the lowest amplitude EEG events (Allen, Josephs and Turner, 2000). The FMRIB plugin uses the FASTR method to remove gradient artifacts (Niazy *et al.*, 2005). The method requires the recording of the scanner trigger at the start of each TR. An average template is computed from the detected TRs and subtracted from the raw EEG data. Following this process, the data is corrected further using principal component analysis (PCA) to reduce residual artifacts. Residual artifacts are further reduced using adaptive noise cancellation (Allen, Josephs and Turner, 2000).

Pulse Artifact/BCG Removal

ECG data collected inside the MRI scanner has a pronounced T wave that increases as the field strength increases (Schmidt *et al.*, 2018). These pulse artifacts The FMRIB plugin identifies QRS events using an algorithm that detects events, aligns them, and corrects for false positives and negatives (Christov, 2004; Kim, Yoon and Park, 2004). From the events, a median signal is computed to create an artifact template, which is subsequently subtracted from the data.

MRI Preprocessing

We used the Connectome Computation System (CCS) to preprocess the MRI/fMRI data (Xu *et al.*, 2015). For the anatomic data, we performed skull stripping using a combination of Brain Extraction Toolbox (BET) and Freesurfer. Data was then segmented (Freesurfer) and registered to a template space (MNI152 2006) using FLIRT and MCFLIRT (Jenkinson and Smith, 2001; Jenkinson *et al.*, 2002). The runs for the fMRI data were all preprocessed equally. Initially, the first five volumes are discarded, then the data is despiked and slice time and motion corrected. The functional data is skull striped with 3dAutomask and refined using the structural data. Functional data is registered to the anatomical images using boundary-based registration based on N4 using Freesurfer). Nuisance correction is done using the Friston 24 motion parameters, average CSF, and WM signals, with/without GSR as regressors. The data is also processed with/without temporal filtering (0.01-0.1Hz) and with/without a 6mm FWHM spatial filter. Time series were extracted from 400 ROIS (Schaefer 400 atlas) to be further processed (Schaefer *et al.*, 2018).

Data Quality Control

<u>EEG</u>

To assess the raw data quality, we followed a similar pipeline described in (Delorme *et al.*, 2022). This approach led to three data quality metrics related to (i) percent of “good” channels, (ii) percent of “good” trials, and (iii) number of independent components (IC) related to brain source activity. The “good” channels are those that remain after the initial preprocessing steps. These initial steps involve removing the channels with more than five seconds of non-activity, more than four high-frequency noise standard deviations, or less than 0.7 in correlation with nearby channels. The “good” trials are related to the data periods that were not contaminated with artifacts (i.e., EMG, movement, and eye blinks). Finally, to identify the ICs belonging to brain source activity, we compute the ICs running RunICA plugin from the EEGLab toolbox. Since the ICA approach is just looking for weighted combinations of channels that produce statistically independent non-Gaussian data distribution and does not handle any physiological information, to evaluate an ICs as coming or not from brain activity, the individual classification of the ICs was performed using the ICLabel plugin from the EEGLab toolbox.

MRI

Temporal measures of fMRI data include: median framewise displacement (Jenkinson *et al.*, 2002), root mean square of the temporal change (DVARS) and temporal signal-to-noise ratio (TSNR).

Statistical Analysis

Multiple permutation testing was performed to look for some statistical relevance that allows identifying differences underlying in EEG data for two conditions, checkerboard and rest condition. Permutation testing is a robust framework for statistical significance assessment in EEG analysis. One of the main advantages of multiple permutation testing is that do not require to have the same number of participants for each condition. The main idea of the permutation testing algorithm is to shuffle the data into two new groups. Then, compute any test statistic, such as a t-test or a correlation coefficient, generating a statistical value. In this work, we calculated the standard deviation unit by subtracting the mean of the null hypothesis distribution from the observed statistic value and dividing it by the standard deviations of the null hypothesis distribution. So, we create a test statistic for each new group based on the shuffle data along one thousand iterations. Finally, a multiple comparison correction was applied. We applied the pixel-based multiple comparisons correction. Correcting for multiple comparisons using pixel-based statistics relies on creating a distribution of the pixel from each iteration of permutation testing with the most extreme statistical value.

Data sharing

Open-access data

There are various neuroimaging databases providing open access datasets such as OpenNeuro (https://openneuro.org), DataDryad (https:/datadryad.org), and Zenodo (https://zenodo.org). Across the available datasets (see Table 2), simultaneous data exists for sleep (Yameng Gu *et*

al., 2022), tasks (Lioi *et al.*, 2019), and resting state data. While there are some EEG-fMRI datasets available, to our knowledge, no open-access datasets are available with naturalistic viewing data. This dataset is more comprehensive, and contains resting state, a visual task paradigm, and naturalistic video stimuli. In our data release, we provide raw and preprocessed data. In addition, physiological data collected concurrently is also provided, including eye tracking, electrooculography, electrocardiography, and respiration rate

Authors	Participants	Task	Scanner	Functional	Head Coil	EEG	Physiology	Notes
Yameng Gu *et al.*, 2022	33 healthy	10m resting state (2 runs); 15m sleep (Varied)	3T Siemens Prisma Fit (Siemens, Erlangen, Germany)	EPI [TR: 2100ms; TE: 25ms; FOV: 240mm; voxel size: 3 × 3 × 4 mm; 35 slices]	20-channel receive-array	Brain Products (32 electrodes)	ECG, EOG	Structural and functional MRI, Raw EEG
Lioi *et al.*, 2019	30 right-handed NF-naïve healthy	6m40s neurofeedback, 5m20s neurofeedback (5 runs)	3T Verio MRI [VB17] (Siemens, Erlangen, Germany)	EPI [TR: 2000ms; TE: 23ms; FOV: 210mm; voxel size: 2 × 2 × 4 mm; 32 slices; no slice gap]	12-channel receiver head coil	-	-	Only 27 of them signed the consent to publish their anonymized data, and were therefore included in the public datasets
Roy *et al.*, 2017	20 healthy	4m42s (5 consecutive 42s trials followed by 12s rest) [2538s (9) - 4794s (14)]	3T Siemens Skyra (Siemens, Erlangen, Germany)	EPI [TR: 2200ms; TE: 30ms; flip angle: 90°; voxel size: 3 × 3 × 3 mm; 36 slices; fat suppression on]	16 channel receive only head coil	BrainProducts (64 electrodes)	ECG	12 preprocessed EEG scan files + 12 preprocessed fMRI scan folders
Robertson *et al.*, 2015	18 healthy (17 right-handed, 1 left-handed; 10 females, 8 males)	multi-source interference task (MSIT)	3T Siemens Verio (Siemens, Erlangen Germany)	EPI [TR: 3000ms; TE: 30ms; flip angle: 90°; matrix size: 64×64; voxel size: 3.2 × 3.2 × 3.2 mm; 30 slices, abutting]	12-channel phased array head coil	Neuroscan (64 electrodes)	ECG, EOG	-
Zumer *et al.*, 2015	16 healthy participants (15 females)	one-back visuospatial working memory task	3T Siemens TIM Trio (Siemens, Erlangen, Germany)	EPI [TR: 2000ms; TE: 6.9, 16.2, 25, 35, 44 ms; flip angle: 80°; matrix size: 64×64; voxel size: 3.5 × 3.5 × 3 mm; 39 slices; acceleration factor: 3]	32-channel head coil	BrainProducts (64 electrodes)	ECG, infrared eye tracker	Polhemus FASTRAK device was used to record the exact location of each EEG electrode on the participant's head relative to three fiducial points
Gherman and Philiastides, 2018	30 healthy (24 used)	perceptual decision task (random dot kinematogram)	3T Siemens TIM Trio (Siemens, Erlangen, Germany)	EPI [TR: 2000ms; TE: 30ms; flip angle: 80°; FOV: 210mm; matrix size: 70×70; voxel size: 3 × 3 × 3 mm; 32 slices, interleaved; 0.3 mm slice gap]	12-channel head coil	BrainProducts (64 electrodes)	ECG	-
Mele *et al.*, 2019	5 healthy	attention task (380 days; range 239–560 days)	3T Philips Achieva (Philips Medical Systems, Best, Netherlands)	EPI [TR: 2000ms; TE: 30ms; flip angle: 90°; matrix size: 80×80; voxel size: 2.75 × 2.75 × 3.75 mm; 36 slices, acquired continuously in ascending order; no slice gap]	32-channel head volume coil	WaveGuard (64 electrodes)	ECG, EOG	-

Authors	Participants	Task	Scanner	Functional	Head Coil	EEG	Physiology	Notes
He *et al.*, 2018	20 participants (12 females)	content judgment task (2 runs, 425 volumes)	3T Siemens TIM Trio (Siemens, Erlangen, Germany)	EPI [TR: 2000ms; TE: 30ms; flip angle: 90°; FOV: 230mm; matrix size: 64×64; voxel size: 3.59 × 3.59 × 4 mm; 30 slices; 0.36mm slice gap]	Unspecified	Brain Products (32 electrodes)	ECG	-
Wirsich *et al.*, 2020	16 subjects using a 64-channel EEG setup in a 1.5T MR-scanner (64Ch-1.5T)	resting state	1.5T Siemens Avanto (Siemens, Erlangen, Germany)	EPI [TR: 2160ms; TE: 30ms; flip angle: 75°; FOV: 210mm; voxel size: 3.3 × 3.3 × 4 mm; 30 slices; 1mm slice gap]	Unspecified	BrainProducts (64 electrodes)	ECG	Only 1.5T available, other data available upon request
Wirsich *et al.*, 2020	26 subjects using a 64-channel	resting state	3T Siemens TIM Trio (Siemens, Erlangen, Germany)	EPI [TR: 2000ms; TE: 50ms; flip angle: 78°; FOV: 192mm; voxel size: 3 × 3 × 3 mm; 40 slices]	Unspecified	BrainProducts (64 electrodes)	ECG, EOG	-
Wirsich *et al.*, 2020	21 subjects using a 256-channel	resting state	3T Siemens TIM Trio, 3T Siemens Prisma (Siemens, Erlangen, Germany)	EPI [TR: 1990ms; TE: 30ms; flip angle: 90°; FOV: 192mm; voxel size: 3 × 3 × 3.75 mm; 32 slices]	Unspecified	Electrical Geodesic (258 electrodes)	2 ECG	-
Wirsich *et al.*, 2020	9 subjects using a 64 channel	resting state	7T Siemens Magnetom [head MR-scanner] (Siemens, Erlangen, Germany)	EPI [TR: 1000ms; TE: 25ms; flip angle: 54°; FOV: 220mm; voxel size: 2.2 × 2.2 × 2.2 mm; 69 slices; acceleration factor: 2; simultaneous multi-slice: 3]	Unspecified	BrainProducts (64 electrodes)	ECG, 4 modified motion	-

Table 2. Open-access simultaneous EEG-fMRI data sets. Simultaneous EEG-fMRI data sets are available from various online repositories on OpenNeuro, DataDryad and Zenodo for sleep, task, and resting state data.

Data privacy

All imaging data in this release has been de-identified, removing any personal identifying information (as defined by the Health Insurance Portability and Accountability) from data files, including facial features. Facial features were removed using the “mri_deface” software package developed by Bischoff-Grethe et al. (Bischoff-Grethe *et al.*, 2007).

Data access

All data can be accessed through the 1,000 Functional Connectomes Project and its International Neuroimaging Data-sharing Initiative (FCP/INDI) based at http://fcon_1000.projects.nitrc.org/indi/eeg_fmri_nat_view.html. This website provides directions for users to directly download all the imaging data from an Amazon Simple Storage Service (S3) bucket. Raw data is stored in the Brain Imaging Data Structure (BIDS) format, which is an increasingly popular approach to describing imaging data in a standard format. Preprocessed data is also provided through the website. Code used for preprocessing the EEG and fMRI data are available at: https://github.com/NathanKlineInstitute/NATVIEW_EEGFMRI

Results

EEG data validation and quality

Figure 1 shows the comparison of EEG during the checkerboard task under the three scan conditions. Figure 1A shows the signal power over 2s epochs during the checkerboard and rest task averaged across subjects. Comparing the checkerboard versus rest condition, the checkerboard shows peaks at 12Hz and 24Hz, representing the driving frequency of the checkerboard and its harmonic, respectively. When moving into the scanner, the power of the checkerboard is reduced. Nonetheless, peaks at 12Hz and 24Hz are still visible in the Scanner OFF and Scanner ON condition. The Scanner ON condition also contains a peak at 18Hz in both rest and checkerboard conditions. This peak denotes residual artifact that is left behind in the signal after the gradient artifact removal step. When looking at the frequency over the duration of the 2s epoch, the difference between the rest and checkerboard condition are evident with the 12Hz driving frequency and the 24Hz harmonic appearing across the entire epoch (Figure 1B). As shown in Figure 1C, these differences are statistically significant. While these plots focus on the Oz electrode, the signal power also extends to other electrodes in the occipital region (Figure 1D).

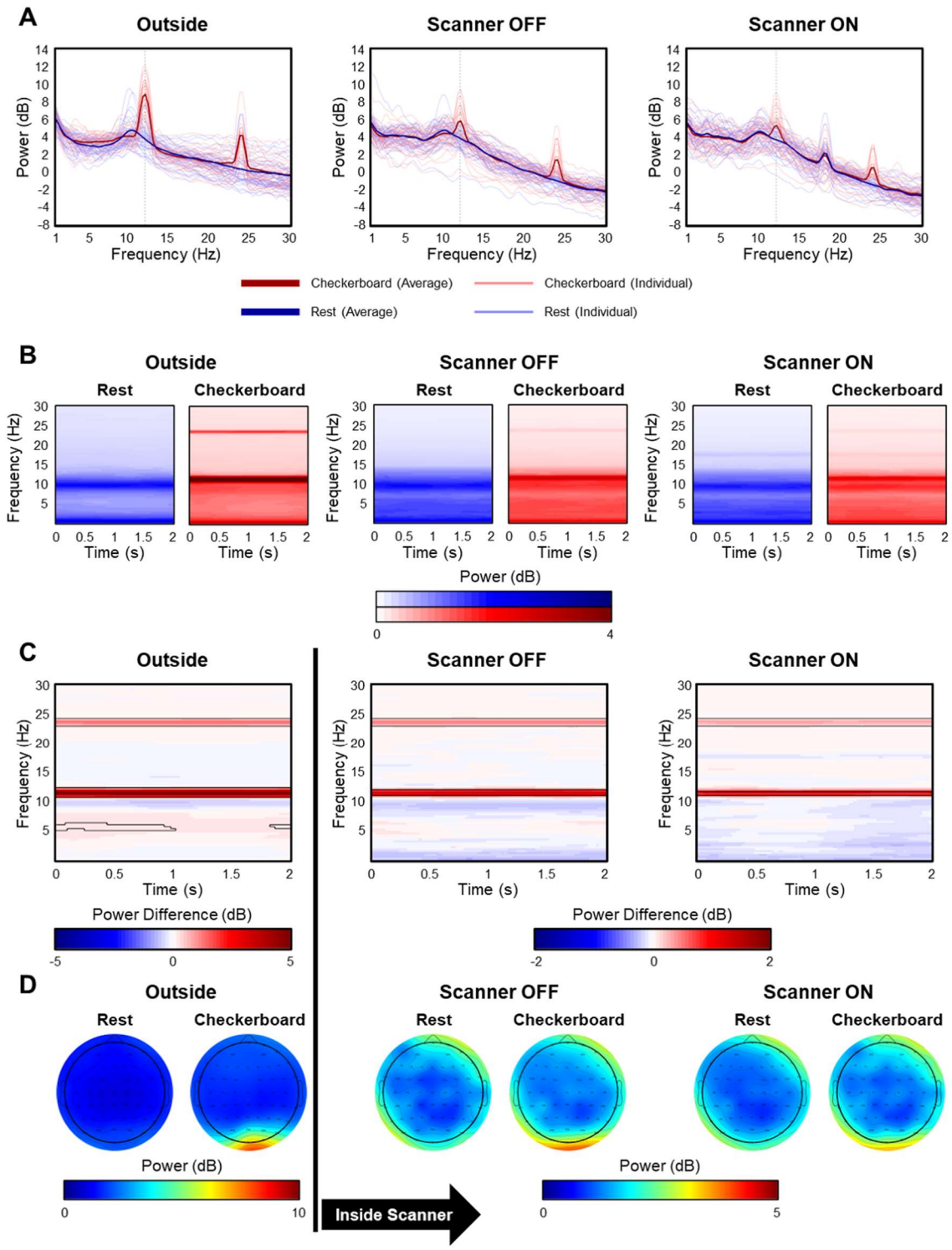

Figure 1. EEG data validation. A) Comparison of power spectrum for participants across conditions: Outside, Scanner OFF, and Scanner ON. B) Time-frequency comparison of checkerboard and rest blocks over 2s epochs across conditions C) Permutation subtraction of Checkerboard and Rest D) Topographic plots comparing Rest and Checkerboard condition across three conditions

As mentioned above, three quality assessment metrics were computed for each raw EEG dataset: percent of "good" channels, percent of "good" trials, and percent of independent components (ICs) related to brain source activity. The higher the value for these quality metrics represents higher data quality. As shown in Figure 2, data quality was high across all subjects for channels and trials. Although the data quality was highest in the outside condition, similarly high results were found for channels and trials in the Scanner OFF and Scanner ON conditions. The percent of putative brain sources based on ICs classification was significantly lower than the percent of "good" channels and trials. Still, there is no final consensus regarding how many ICs from EEG data must be associated with brain activity. An ideal result might look like exceptionally clean EEG data with an alert research participant. This ideal data would contain minimal ICs unrelated to putative brain activity (e.g., eye blinks). However, in practice, the number of ICs related to brain activity from good quality EEG data is around eighteen ICs regardless of EEG electrode density. In this study, we do not include a rigorous approach to determine the ideal percentage of ICs for a given electrode density from good-quality EEG data. Therefore, the percentage of ICs associated with brain sources is computed based on the total amount of channels. Accordingly, a higher percentage of brain sources is certainly better as evidenced in the comparison across scan conditions. In our judgment, the quality of this dataset is high as the level of quality remains high across scan conditions (Figure 3).

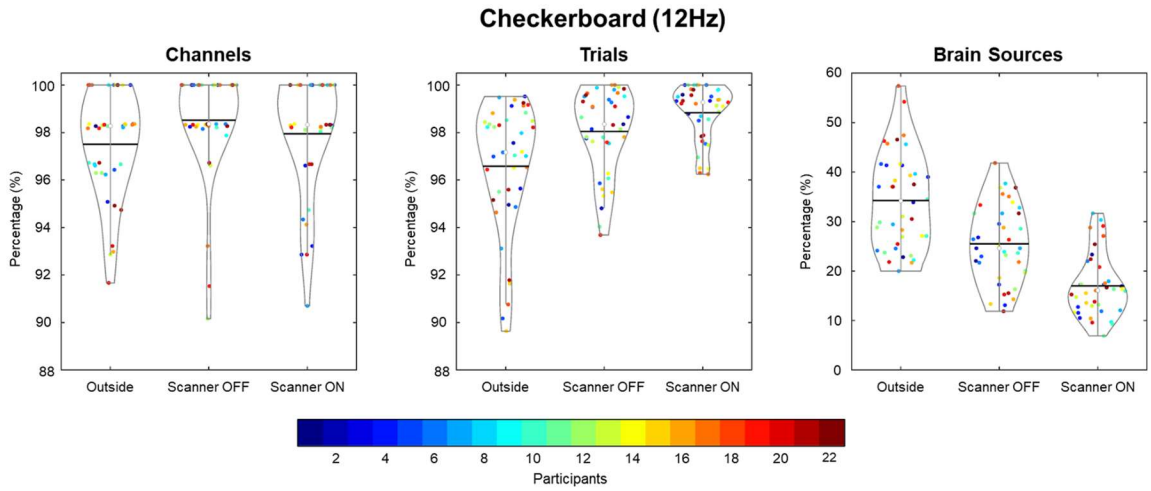

Figure 2. EEG data quality comparison for flickering checkerboard task across participants. Three quality metrics (channels, trials and brain sources) were assessed across scan conditions. For channels and trials, the data quality was high across all scan conditions, denoting high quality of EEG data.

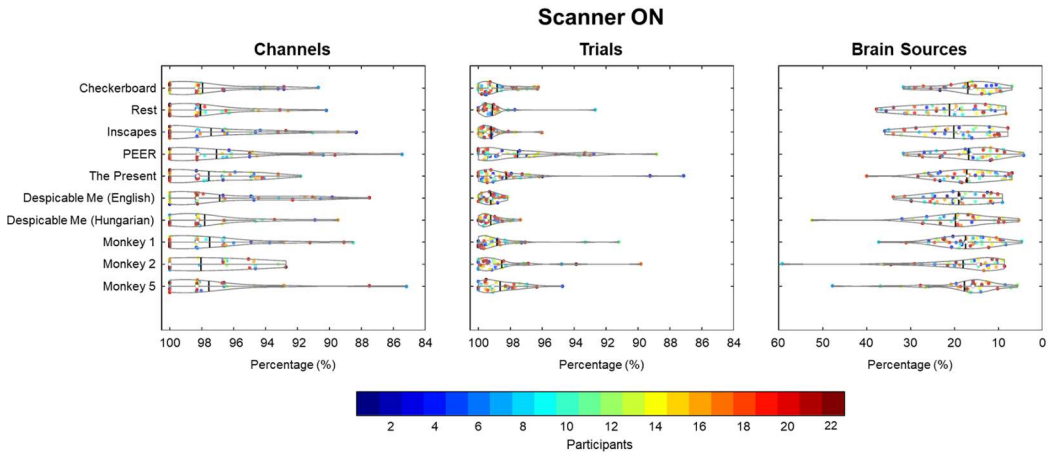

Figure 3. EEG data quality comparison inside scanner. Three quality metrics (channels, trials and brain sources) were assessed across scan conditions. For channels and trials, the data quality was high across all scan conditions, denoting high quality of EEG data.

fMRI data quality

To assess the quality of fMRI data, median framewise displacement (FD) was measured for all scans. As shown in Figure 4, the median FD was for every fMRI scan; scans with a value above 0.2 were considered high motion. To determine if there was an ordering effect, scan sessions were color coded to determine if participants moved more earlier or later in the scan. Most subject data was below the 0.2 threshold (93% of scans) and there was no pattern of ordering across participants.

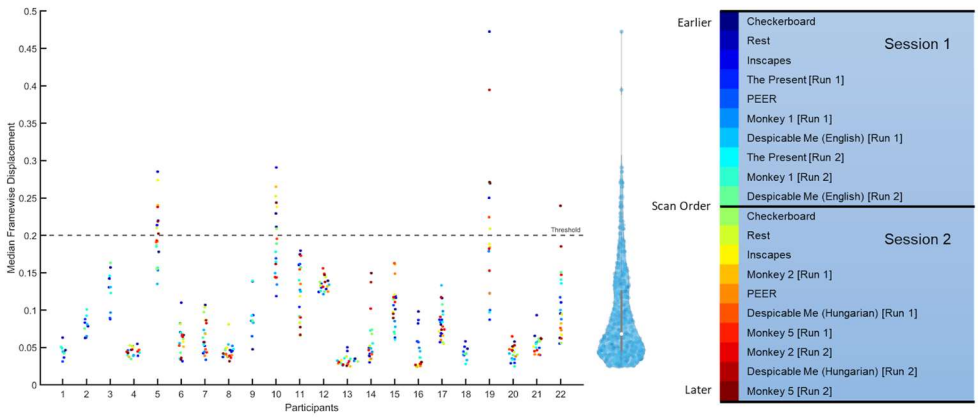

Figure 4. Median framewise displacement for fMRI data. The median framewise displacement was measured for each scan across both sessions and plotted for each participant. Scans with a value above 0.2 were considered high motion, indicated as points about the dotted threshold line. To the right of the plot, is the distribution of all scans. As seen in the distribution, most scans had low motion as measured by median FD.

Multimodal quality data correlations

Values for EEG and MRI data were compared within and between modalities across several quality metrics: mean FD (framewise displacement), median FD, DVARS (temporal derivative of time courses), and tSNR (temporal signal-to-noise ratio) for MRI; channels, trials and brain sources for EEG (Figure 5). Using Spearman's ρ between each modality, shows a strong positive correlation between mean and median FD, and a strong negative correlation between FD measures and tSNR. A weak correlation was found for DVARS and tSNR, but no association was found with DVARS and other measures. For EEG measures, there was no correlation between the different quality measures. Moreover, there was no correlation between quality measures between imaging modalities.

For the checkerboard task, we looked at the correlation between ROIs within subject and between subjects (Figure 6). The large-scale correlation matrix showed stronger within scan correlations than between scans. Of note was the distributions for within scan and within subjects showed a broader distribution of values, with higher correlations for within scan and within subject distributions.

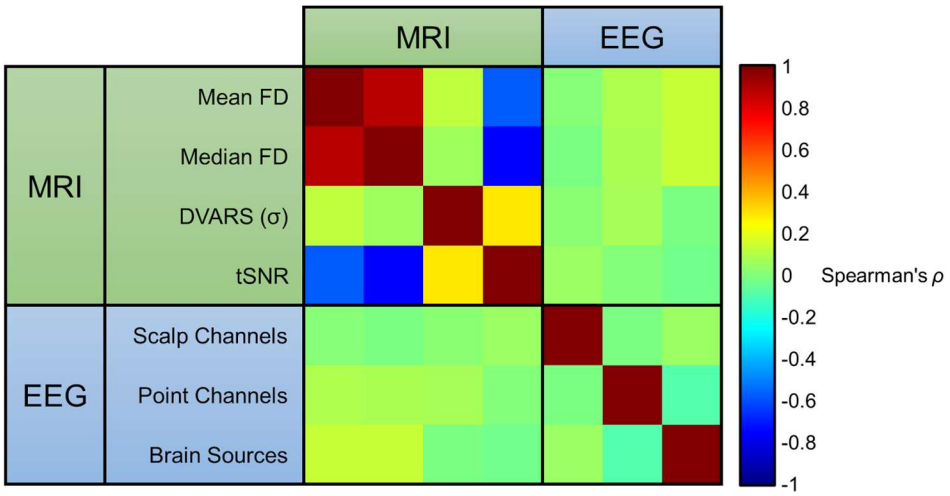

Figure 5. Correlation between MRI and EEG data. There is strong positive correlation between measures of mean and median FD; likewise, there is a strong negative correlation between measures of FD and tSNR. In contrast, there appears no association among EEG measures within modality and with fMRI quality measures.

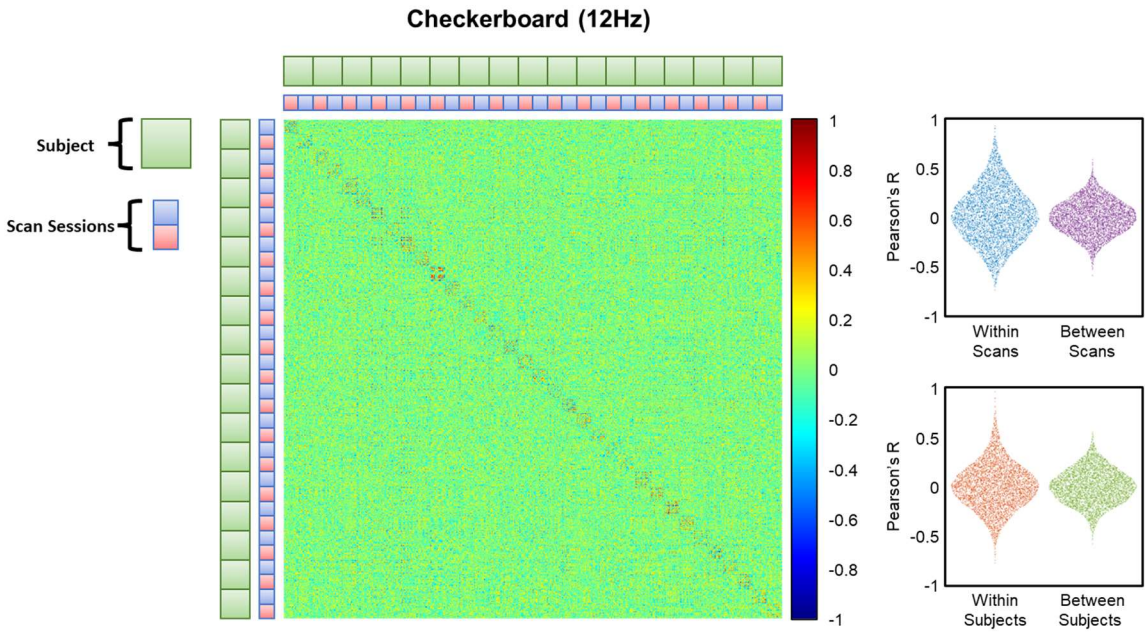

Figure 6. Similarity of full-brain connectivity matrices across subjects (green), sessions (blue/red) as measured using Pearson correlation coefficient. Also depicted is the distributions of correlation coefficients when comparing within scans and between scans from the same subject (within subject), and within subject and between subject scans.

Multimodal data integration

As a multimodal data integration test, we evaluated if by using the EEG signal we are able to predict the hemodynamic response. Specifically, for the flickering checkerboard experiment, after preprocessing, the EEG signal from Oz signal was averaged across participants. This signal was then bandpass filtered (20th order IIR filter between 11Hz and 13Hz), modulated, and convolved with an ideal hemodynamic response function (using a gamma variate function). For each participant, this signal was used as a regressor to map out the BOLD activity. A one-sample t-test was performed to calculate a group activity map (Figure 7A). For comparison purposes, a regressor based on an ideal block design convoluted a gamma variate function was also calculated to look at group level activity using a more traditional approach (Figure 7B). Activity maps shown in Figure 7 indicate that both approaches generate a similar level of activity in the occipital lobe.

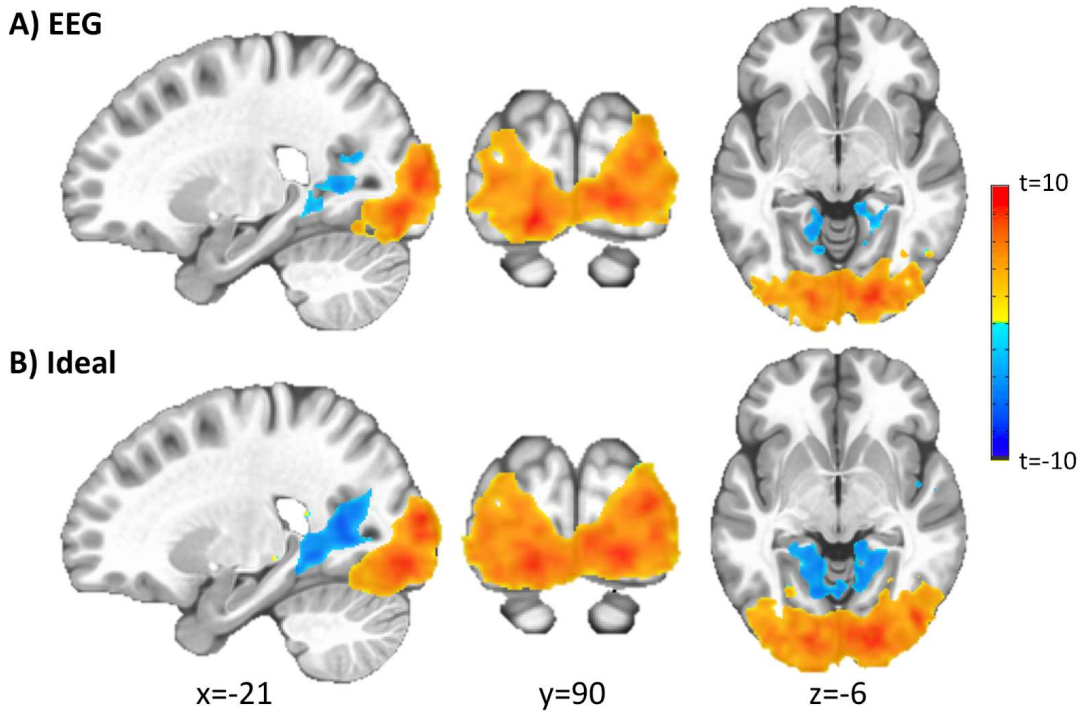

Figure 7. Checkerboard task activation map either using the A) group average EEG signal from Oz as a regressor or B) an ideal hemodynamic response function.

Technical challenges

To collect EEG and fMRI simultaneously requires several methodological considerations. While EEG and fMRI have a long-established history, collecting EEG inside the MRI scanner is challenging for several technical reasons. The main problem encountered when collecting a functional recording is the generation of artifacts from various sources. The main artifact arises from the gradient artifact generated during echo-planar imaging (EPI), which induces changes in the magnetic field (Ritter and Villringer, 2006). Another source of noise arises from the scanner environment. While not a problem in all scanners, vibrations from the helium compressor in Siemens Trio and Verio scanners introduce artifacts into the EEG signal (Nierhaus *et al.*, 2013); these vibrations induce non-stationary artifacts that contaminate the EEG signal. Yet another source of noise is caused by the pulsation of arteries in the scalp that cause movement in EEG electrodes and generation voltage. The source of noise, the ballistocardiogram (BCG) signal, captures the ballistic forces of blood in the cardiac cycle (Yan *et al.*, 2009; Luo, Huang and Glover, 2014) and becomes more pronounced as the magnetic field strength increases (Neuner *et al.*, 2014). In addition to a more pronounced signal, the ECG signal can impact data collection and preprocessing. In some cases, the pronounced ECG signal leads to saturation of the signal during the MRI scan sequence. Consequently, this saturation causes signal clipping that can impede QRS detection and pulse artifact removal methods in preprocessing. In this data

release, there are occasions of signal clipping of the ECG channel. For participants where QRS detection of the ECG channel failed, one method used in this study was to perform QRS detection on every EEG channel and select the channel containing the mode of the detected QRS complexes. From this channel, the median template is created and applied to across channels for pulse artifact removal.

To address these numerous sources of noise, there are several techniques. Gradient artifacts can be minimized by modifying the configuration or layout of EEG leads (Ferreira *et al.*, 2016) There are several approaches to reduce or remove gradient artifacts. To remove the gradient field artifact, we use the MR clock to record the scanner trigger at every TR (Negishi *et al.*, 2004; Ritter *et al.*, 2007). Using a template artifact subtraction method (Hashimoto, Elder and Vitek, 2002), gradient artifact is recorded at each TR onset and averaged to create a template. The template is then subtracted from the signal to produce a clean signal. In this study, we used the MRIB plug-in for EEGLAB, provided by the University of Oxford Centre for Functional MRI of the Brain (FMRIB), to regress the MRI gradient artifact (Iannetti *et al.*, 2005; Niazy *et al.*, 2005). For noise induced by the helium compressor, there are methods for recording and regressing these motion induced artifacts (Abbott *et al.*, 2015; van der Meer *et al.*, 2016); however, in our experiments, the simplest method for removing this artifact was to turn off the helium compressor during simultaneous recordings. While there is a risk of helium boiling off a temperature rise in the scanner, this can be addressed by having shorter scan sessions. In our study, temperatures of the cooling system did not fluctuate greatly. While shorter scans are ideal, we collected data upwards of 2 hours without issue.

Another factor that was found to impact the signal, particularly related to signal clipping, was the cable placement inside the scanner. In MR imaging, magnetic homogeneity is a major component of MRI system design. Maintaining the magnetic field at the center of the scanner, or isocenter, helps to produce high quality images. Magnetic field homogeneity is further improved with magnetic shimming. Nonetheless, objects aligned at the center of the bore have higher image quality than objects away from the center of the bore. In our simultaneous EEG-fMRI recordings, cable placement greatly affected EEG data quality. For cable placement, several factors must be taken into consideration. When scanning, researchers must ensure their setup minimizes loops and cables should run along the center of the bore to ensure data quality (Ritter and Villringer, 2006). Excessive bends or loops in wires can induce current in cables, thus introducing artifacts into the EEG signal. In our experiments, cables from the EEG cap were run through the head coil above the participant's head and taped along the center of the bore to minimize movement and to ensure optimal position in the scanner. One way to minimize issues with cables in the scanner is to minimize the cable length between the cap and amplifiers. All major scanner vendors offer head coils that are designed with a channel for EEG cables that lie directly above a participant's head (Brain Products, 2020). In addition, cables that are bundled produce less artifacts than ribboned cables (Chowdhury, Mullinger and Bowtell, 2015).

Concluding remarks

Simultaneous EEG and fMRI offers rich data that provides complimentary temporal and spatial information. Here, we demonstrated consistency of EEG results outside and inside the scanner. These analyses also indicate the utility of EEG-informed analyses that can provide fMRI that are data-driven. Additionally, the main benefit of this release is offering a rich resource of naturalistic viewing (Inscapes and movie clips), resting state data and task data (checkerboard), that to our knowledge, has not been available previously. This resource can also be used by investigators to optimize data processing pipelines and explore secondary analyses. Finally, this data release continues the trends of open data initiatives that provides transparency, efficiency and an indispensable community resource.

Funding

Primary support for the work by is provided by the BRAIN Initiative (R01MH111439) and CONTE center (P50MH109429) grants from the NIH. Data hosting is supported by AWS's Open Data program.

References

- Abbott, D.F. *et al.* (2015) 'Constructing carbon fiber motion-detection loops for simultaneous EEG–fMRI', *Frontiers in Neurology*, 5. Available at: https://www.frontiersin.org/article/10.3389/fneur.2014.00260 (Accessed: 22 March 2022).

- Alexander, L.M. *et al.* (2017) 'An open resource for transdiagnostic research in pediatric mental health and learning disorders', *Scientific Data*, 4(1), p. 170181. Available at: https://doi.org/10.1038/sdata.2017.181.

- Allen, P.J., Josephs, O. and Turner, R. (2000) 'A method for removing imaging artifact from continuous EEG recorded during functional MRI', *NeuroImage*, 12(2), pp. 230–239. Available at: https://doi.org/10.1006/nimg.2000.0599.

- Bayram, A. *et al.* (2016) 'Achromatic temporal-frequency responses of human lateral geniculate nucleus and primary visual cortex', *Vision Research*, 127, pp. 177–185. Available at: https://doi.org/10.1016/j.visres.2016.09.001.

- Bischoff-Grethe, A. *et al.* (2007) 'A technique for the deidentification of structural brain MR images', *Human Brain Mapping*, 28(9), pp. 892–903. Available at: https://doi.org/10.1002/hbm.20312.

- Brain Products (2020) *Changes to the Brain Products standard BrainCap MR*, *Brain Products Press Release*. Available at: https://pressrelease.brainproducts.com/braincap_mr/ (Accessed: 23 March 2022).

- Buysse, D.J. *et al.* (1989) 'The Pittsburgh Sleep Quality Index: a new instrument for psychiatric practice and research', *Psychiatry Res*, 28(2), pp. 193–213. Available at: https://doi.org/10.1016/0165-1781(89)90047-4.

- Chowdhury, M.E.H., Mullinger, K.J. and Bowtell, R. (2015) 'Simultaneous EEG-fMRI: evaluating the effect of the cabling configuration on the gradient artefact', *Physics in Medicine and Biology*,

60(12), pp. N241-250. Available at: https://doi.org/10.1088/0031-9155/60/12/N241.

- Christov, I.I. (2004) ‘Real time electrocardiogram QRS detection using combined adaptive threshold’, *Biomedical Engineering Online*, 3(1), p. 28. Available at: https://doi.org/10.1186/1475-925X-3-28.

- Delorme, A. *et al.* (2022) ‘NEMAR: An open access data, tools, and compute resource operating on NeuroElectroMagnetic data’. arXiv. Available at: https://doi.org/10.48550/arXiv.2203.02568.

- Delorme, A. and Makeig, S. (2004) ‘EEGLAB: an open source toolbox for analysis of single-trial EEG dynamics including independent component analysis’, *Journal of Neuroscience Methods*, 134(1), pp. 9–21. Available at: https://doi.org/10.1016/j.jneumeth.2003.10.009.

- Egan, M.K. *et al.* (2021) ‘Safety and data quality of EEG recorded simultaneously with multi-band fMRI’, *PLOS ONE*, 16(7), p. e0238485. Available at: https://doi.org/10.1371/journal.pone.0238485.

- Ferreira, J.L. *et al.* (2016) ‘Gradient Artefact Correction and Evaluation of the EEG Recorded Simultaneously with fMRI Data Using Optimised Moving-Average’, *Journal of Medical Engineering*, 2016, p. 9614323. Available at: https://doi.org/10.1155/2016/9614323.

- Frey, J. (2014) *The Present*. Available at: https://www.youtube.com/watch?v=C_nJJHaNmnY (Accessed: 22 February 2022).

- Galloway, N.R. (1990) ‘Human Brain Electrophysiology: Evoked Potentials and Evoked Magnetic Fields in Science and Medicine’, *The British Journal of Ophthalmology*, 74(4), p. 255.

- Gherman, S. and Philiastides, M.G. (2018) ‘Data from: Human VMPFC encodes early signatures of confidence in perceptual decisions’. Dryad. Available at: https://doi.org/10.5061/DRYAD.3DN0045.

- Hashimoto, T., Elder, C.M. and Vitek, J.L. (2002) ‘A template subtraction method for stimulus artifact removal in high-frequency deep brain stimulation’, *Journal of Neuroscience Methods*, 113(2), pp. 181–186. Available at: https://doi.org/10.1016/s0165-0270(01)00491-5.

- He, X. *et al.* (2018) ‘Disrupted dynamic network reconfiguration of the language system in temporal lobe epilepsy’, *Brain*, 141(5), pp. 1375–1389. Available at: https://doi.org/10.1093/brain/awy042.

- Herrmann, C.S. (2001) ‘Human EEG responses to 1-100 Hz flicker: resonance phenomena in visual cortex and their potential correlation to cognitive phenomena’, *Experimental Brain Research*, 137(3–4), pp. 346–353. Available at: https://doi.org/10.1007/s002210100682.

- Iannetti, G.D. *et al.* (2005) ‘Simultaneous recording of laser-evoked brain potentials and continuous, high-field functional magnetic resonance imaging in humans’, *NeuroImage*, 28(3), pp. 708–719. Available at: https://doi.org/10.1016/j.neuroimage.2005.06.060.

- Jenkinson, M. *et al.* (2002) ‘Improved optimization for the robust and accurate linear registration and motion correction of brain images’, *NeuroImage*, 17(2), pp. 825–841. Available at: https://doi.org/10.1016/s1053-8119(02)91132-8.

- Jenkinson, M. and Smith, S. (2001) ‘A global optimisation method for robust affine registration of brain images’, *Medical Image Analysis*, 5(2), pp. 143–156. Available at: https://doi.org/10.1016/s1361-8415(01)00036-6.

- Kim, K.H., Yoon, H.W. and Park, H.W. (2004) ‘Improved ballistocardiac artifact removal from the

electroencephalogram recorded in fMRI', *Journal of Neuroscience Methods*, 135(1–2), pp. 193–203. Available at: https://doi.org/10.1016/j.jneumeth.2003.12.016.

- Lioi, G. *et al.* (2019) *Simultaneous MRI-EEG during a motor imagery neurofeedback task: an open access brain imaging dataset for multi-modal data integration*. preprint. Neuroscience. Available at: https://doi.org/10.1101/862375.

- Luo, Q., Huang, X. and Glover, G.H. (2014) 'Ballistocardiogram Artifact Removal with a Reference Layer and Standard EEG Cap', *Journal of neuroscience methods*, 233, pp. 137–149. Available at: https://doi.org/10.1016/j.jneumeth.2014.06.021.

- Mantini, D. *et al.* (2012) 'Interspecies activity correlations reveal functional correspondence between monkey and human brain areas', *Nature Methods*, 9(3), pp. 277–282. Available at: https://doi.org/10.1038/nmeth.1868.

- van der Meer, J.N. *et al.* (2016) 'Carbon-wire loop based artifact correction outperforms post-processing EEG/fMRI corrections--A validation of a real-time simultaneous EEG/fMRI correction method', *NeuroImage*, 125, pp. 880–894. Available at: https://doi.org/10.1016/j.neuroimage.2015.10.064.

- Mele, G. *et al.* (2019) 'Simultaneous EEG-fMRI for functional neurological assessment', *Frontiers in Neurology*, 10. Available at: https://www.frontiersin.org/article/10.3389/fneur.2019.00848 (Accessed: 21 February 2022).

- Negishi, M. *et al.* (2004) 'Removal of time-varying gradient artifacts from EEG data acquired during continuous fMRI', *Clinical Neurophysiology*, 115(9), pp. 2181–2192. Available at: https://doi.org/10.1016/j.clinph.2004.04.005.

- Neuner, I. *et al.* (2014) 'Simultaneous EEG–fMRI acquisition at low, high and ultra-high magnetic fields up to 9.4T: Perspectives and challenges', *NeuroImage*, 102, pp. 71–79. Available at: https://doi.org/10.1016/j.neuroimage.2013.06.048.

- Niazy, R.K. *et al.* (2005) 'Removal of FMRI environment artifacts from EEG data using optimal basis sets', *NeuroImage*, 28(3), pp. 720–737. Available at: https://doi.org/10.1016/j.neuroimage.2005.06.067.

- Nierhaus, T. *et al.* (2013) 'Internal ventilation system of MR scanners induces specific EEG artifact during simultaneous EEG-fMRI - PubMed', *NeuroImage* [Preprint]. Available at: https://pubmed.ncbi.nlm.nih.gov/23435207/ (Accessed: 22 March 2022).

- Park, S.H. *et al.* (2017) 'Functional Subpopulations of Neurons in a Macaque Face Patch Revealed by Single-Unit fMRI Mapping', *Neuron*, 95(4), pp. 971-981.e5. Available at: https://doi.org/10.1016/j.neuron.2017.07.014.

- Park, S.H. *et al.* (2022) 'Parallel functional subnetworks embedded in the macaque face patch system', *Science Advances*, 8(10), p. eabm2054. Available at: https://doi.org/10.1126/sciadv.abm2054.

- Ritter, P. *et al.* (2007) 'Evaluating gradient artifact correction of EEG data acquired simultaneously with fMRI', *Magnetic Resonance Imaging*, 25(6), pp. 923–932. Available at: https://doi.org/10.1016/j.mri.2007.03.005.

- Ritter, P. and Villringer, A. (2006) 'Simultaneous EEG–fMRI', *Neuroscience & Biobehavioral Reviews*, 30(6), pp. 823–838. Available at: https://doi.org/10.1016/j.neubiorev.2006.06.008.

- Robertson, J.A. *et al.* (2015) 'Data from: Simultaneous fMRI and EEG during the multi-source

interference task'. Dryad. Available at: https://doi.org/10.5061/DRYAD.C1M3B.

- Roy, A.V. *et al.* (2017) 'Data from: Deactivation in the posterior mid-cingulate cortex reflects perceptual transitions during binocular rivalry: evidence from simultaneous EEG-fMRI'. Dryad. Available at: https://doi.org/10.5061/DRYAD.BF1B1.

- Russ, B.E. and Leopold, D.A. (2015) 'Functional MRI mapping of dynamic visual features during natural viewing in the macaque', *NeuroImage*, 109, pp. 84–94. Available at: https://doi.org/10.1016/j.neuroimage.2015.01.012.

- Schaefer, A. *et al.* (2018) 'Local-Global Parcellation of the Human Cerebral Cortex from Intrinsic Functional Connectivity MRI', *Cerebral Cortex (New York, N.Y.: 1991)*, 28(9), pp. 3095–3114. Available at: https://doi.org/10.1093/cercor/bhx179.

- Schmidt, M. *et al.* (2018) 'Filtering of ECG signals distorted by magnetic field gradients during MRI using non-linear filters and higher-order statistics', *Biomedical Engineering / Biomedizinische Technik*, 63(4), pp. 395–406. Available at: https://doi.org/10.1515/bmt-2016-0232.

- Son, J. *et al.* (2020) 'Evaluating fMRI-Based Estimation of Eye Gaze During Naturalistic Viewing', *Cerebral Cortex*, 30(3), pp. 1171–1184. Available at: https://doi.org/10.1093/cercor/bhz157.

- SR Research Ltd. (2009) 'EyeLink 1000 User Manual'. Available at: http://sr-research.jp/support/EyeLink%201000%20User%20Manual%201.5.0.pdf (Accessed: 15 March 2022).

- Sun, P. *et al.* (2014) 'BOLD Signal Change and Contrast Reversing Frequency: An Event-Related fMRI Study in Human Primary Visual Cortex', *PLoS ONE*, 9(6), p. e99547. Available at: https://doi.org/10.1371/journal.pone.0099547.

- Vanderwal, T. *et al.* (2015) 'Inscapes: a movie paradigm to improve compliance in functional magnetic resonance imaging', *NeuroImage*, 122, pp. 222–232. Available at: https://doi.org/10.1016/j.neuroimage.2015.07.069.

- Wirsich, J. *et al.* (2020) 'The relationship between EEG and fMRI connectomes is reproducible across simultaneous EEG-fMRI studies from 1.5T to 7T'. Zenodo. Available at: https://doi.org/10.5281/zenodo.3905103.

- Xu, T. *et al.* (2015) 'A Connectome Computation System for discovery science of brain', *Science Bulletin*, 60(1), pp. 86–95. Available at: https://doi.org/10.1007/s11434-014-0698-3.

- Yameng Gu *et al.* (2022) 'Simultaneous EEG and fMRI signals during sleep from humans'. Openneuro. Available at: https://doi.org/10.18112/OPENNEURO.DS003768.V1.0.3.

- Yan, W.X. *et al.* (2009) 'Physical modeling of pulse artefact sources in simultaneous EEG/fMRI', *Human Brain Mapping*, 31(4), pp. 604–620. Available at: https://doi.org/10.1002/hbm.20891.

- Zumer, J.M. *et al.* (2015) 'Data from: Occipital alpha activity during stimulus processing gates the information flow to object-selective cortex'. Dryad. Available at: https://doi.org/10.5061/DRYAD.2HR38.